Journal of Marine Research, 54, 605–630, 1996

Journal of
MARINE RESEARCH

Volume 54, Number 4

The solubility pump of carbon in the subtropical gyre of the North Atlantic

by Michael J. Follows[1], Richard G. Williams[2] and John C. Marshall[1]

ABSTRACT

The subduction of carbon is examined using abiotic models of the solubility pump in the subtropical gyre of the North Atlantic. The importance of the seasonal cycle of the mixed layer, and advection of carbon, is examined using sensitivity experiments with a Lagrangian model of the carbon system. The rate of subduction of carbon is found to be strongly influenced by the gradients in mixed-layer thickness over the gyre and, to a lesser extent, modified by the end of winter bias in the properties of subducted fluid.

A seasonally-cycling geochemical model of the carbon system is then developed for the North Atlantic. The model is diagnosed to examine the seasonal exchange in carbon between the atmosphere and ocean induced by the seasonal warming and cooling. There is a net annual air-sea flux of carbon into the subtropical gyre of the model due to undersaturation of p_{CO_2} with respect to the local equilibrium with the atmosphere. The undersaturation is due to advection of carbon by the circulation. Along the path of the Gulf Stream, northward advection and cooling of the low latitude waters is so rapid that the surface waters are significantly undersaturated in carbon. Due to its long equilibration period, there is a resultant air-sea flux of carbon dioxide over the northern flank and interior of the subtropical gyre. Warm, low carbon water from the tropics is fluxed into the southern flank of the subtropical gyre in the Ekman layer, inducing an oceanic uptake of carbon there. The model experiments suggest that it is necessary to account for advection to close the carbon budget in the observed time-series measurements at Bermuda.

1. Introduction

The carbon cycle in the ocean involves a complicated interplay of physical, chemical and biological processes. Observations of the ocean carbon system, such as those gathered

1. Center for Meteorology and Physical Oceanography, MIT, Cambridge, Massachusetts, 02139, U.S.A.
2. Oceanography Laboratories, University of Liverpool, Liverpool, United Kingdom.

during the GEOSECS, TTO, and JGOFS programs, have provided a large-scale description of that system. However, the spatial and temporal resolution available at present is insufficient to completely define the interactions occurring in such a complex, transient system. JGOFS time-series at Hawaii and Bermuda (Winn *et al.*, 1994; Michaels *et al.*, 1994) provide high temporal resolution, but are unable to close the carbon budget, probably due to the neglect of horizontal advection, though uncertainties in sediment trap data provide another possible source of discrepancy (Michaels *et al.*, 1994). Biogeochemical models provide a tool to help understand the observations and the sensitivities of the carbon system; for example, see the annual-mean global integrations by Bacastow and Maier-Reimer (1990) and Sarmiento *et al.* (1992).

In this study we focus on the role of gyre dynamics and seasonality in modulating the inorganic carbon cycle of an abiotic ocean using a hierarchy of models. In particular, we focus on understanding how the dynamics controls the ocean uptake of CO_2 in the subtropical gyres and high latitudes, and the expulsion of CO_2 in the warm tropical regions, which is suggested in the data analysis of Tans *et al.* (1990).

The net air-sea exchange of CO_2 in the gyre is influenced by advection of carbon, as it controls how close the surface waters approach a *local* equilibrium with the overlying atmosphere. Our study investigates how the rapid geostrophic flow in the Gulf Stream prevents a local equilibrium being achieved and subsequently modifies the carbon balance over the interior of the subtropical gyre. Likewise the role of the lateral Ekman fluxes is examined in controlling the carbon transfer between gyres. This dynamical control is discussed in the light of time series observations at Bermuda and Hawaii (Michaels *et al.*, 1994; Winn *et al.*, 1994).

The seasonal cycle has not hitherto been thought to play a significant role in the solubility pump of carbon, since equilibration timescales between mixed-layer and atmospheric partial pressures of CO_2 are of the order of a year or more (Broecker and Peng, 1982). However, the physical properties of the main thermocline *are* sensitive to the seasonal cycle of the mixed layer. The rate of subduction into the main thermocline depends on the vertical and lateral transfer through the mixed layer which has its greatest slope at the end of winter (Marshall *et al.*, 1993). The seasonal cycle leads to a biased transfer into the main thermocline (Stommel, 1979; Williams *et al.*, 1995), as revealed by the *T/S* signature of the main thermocline which matches that of the mixed-layer at the end of winter (Iselin, 1939). Here we explore the implications for the solubility pump of carbon.

In Section 2, a Lagrangian upper ocean model which incorporates relevant physical and chemical processes is used to illustrate mechanisms controlling the solubility pump in the subtropical gyre. In Section 3, a geochemical model of the North Atlantic is then developed, using off-line velocity fields from the 1.0° × 1.2° coupled mixed layer/primitive equation model of the US Community Modeling Effort (CME). The dynamical control of the air-sea fluxes of CO_2 and solubility pump are examined using nonadvective and advective experiments with the seasonally-cycling geochemical model. In Section 4,

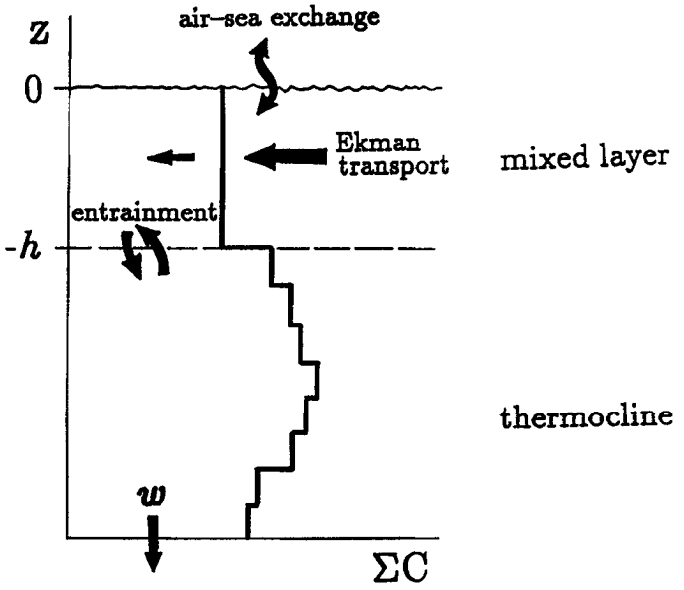

Figure 1. Schematic diagram of the Lagrangian column model following the geostrophic flow. The model solves for the evolution of the vertical distribution of dissolved inorganic carbon, ΣC, in the upper 500 m of the subtropical gyre. Air-sea fluxes of CO_2 are parameterized, and the vertical structure is set by the movement of the mixed layer base and vertical advection. The mixed layer is assumed at all times vertically homogeneous with respect to physical and chemical properties. There is a horizontal convergence of the Ekman velocity in the mixed-layer leading to a vertical velocity at its base.

the JGOFS time series observations at Bermuda and Hawaii are briefly discussed in the light of the processes revealed by the models.

2. Lagrangian studies of the inorganic carbon cycle in the subtropical gyre

a. Lagrangian model of the inorganic carbon cycle

The subduction mechanism may be clearly understood by considering the migration of a column of water as it circuits the gyre (Woods, 1985). Xu (1990) and Xu and Green (1996) have used this Lagrangian frame to model the oceanic carbon cycle in the Gulf Stream system. Following these studies, we choose to examine the carbon cycle follow a water column as it is swept around a subtropical gyre, as sketched schematically in Figure 2(a). The column consists of a vertically homogeneous mixed layer overlying an inviscid, stratified thermocline. For simplicity, the column is assumed to be advected by a current with no vertical shear and to complete a circuit of the subtropical gyre every twelve years. Carbon is fluxed through the sea surface, entrained from the underlying thermocline through the base of the column and undergoes chemical transformations within the column (see schematic, Fig. 1).

More specifically, the dissolved inorganic carbon,[3] ΣC, in the water column is assumed to evolve through vertical advection and turbulent fluxes originating from surface forcing and entrainment—see Figure 1:

$$\frac{D}{Dt}\Sigma C + w\frac{\partial}{\partial z}\Sigma C + \frac{\partial}{\partial z}\overline{w'\Sigma C'} = 0. \tag{1}$$

Here, the Lagrangian derivative is denoted by $D/Dt = \partial/\partial t + \mathbf{u}.\nabla$ and $\mathbf{u}$ is the background horizontal velocity advecting the water column. Integrating (1) from the surface at $z = 0$ over the mixed layer of thickness h, within which properties are, by definition, vertically uniform, gives the evolution of ΣC in the mixed layer:

$$h\frac{D}{Dt}\Sigma C_m + \overline{w'\Sigma C'}_{z=0} - \overline{w'\Sigma C'}_{z=-h} = 0. \tag{2a}$$

After parameterizing the surface and entrainment turbulent fluxes we obtain:

$$h\frac{D}{Dt}\Sigma C_m = k_0 v_e(p^{\text{atm}}_{CO_2} - p_{CO_2}) - \wedge\left(w + \frac{Dh}{Dt}\right)(\Sigma C_m - \Sigma C_{th}), \tag{2b}$$

where subscripts m and th denote the mixed-layer and thermocline, respectively. The flux of ΣC through the surface (first term on the right of (2b)) is parameterized in terms of the difference in p_{CO_2} between the atmosphere and ocean. The oceanic partial pressure, p_{CO_2}, is a function of the concentration of dissolved CO_2, which is dependent on the chemical balance between the component species of dissolved organic carbon. The partition of the ΣC into its bicarbonate, carbonate and dissolved CO_2 forms is determined using a chemical scheme following Hoffert *et al.* (1979), and is a function of the ambient temperature, salinity and alkalinity (see Appendix 1). The chemical scheme is closed by supposing that the surface alkalinity depends only on the salinity, and uses the empirical linear relation of Brewer *et al.* (1986a). The solubility of CO_2, k_0, is also a function of temperature and salinity (Weiss, 1974), and v_e is the piston velocity which here, for clarity, is assumed to be a uniform 20 cm hour^{-1}.

The entrainment of ΣC into the mixed layer (second term on the right of (2b)) from the underlying, stratified fluid is computed as the product of the change in ΣC across the mixed-layer base and the entrainment rate. The entrainment rate is the sum of two terms, the rate of mixed-layer deepening, Dh/Dt, and the vertical advection w (following Denman, 1973). The Heaviside function, $\wedge$, switches the entrainment on or off; $\wedge = 1$ if $w + Dh/Dt > 0$, otherwise it is 0. Note that the vertical advection term in (1) does not contribute within the vertically homogeneous mixed layer, but is nonzero at the base of the mixed layer.

Separating the terms in (2b) into geostrophic and Ekman components, and following a column that moves with the geostrophic flow, the governing equation for the dissolved

3. Dissolved inorganic carbon, $\Sigma C = CO_2 + HCO_3^- + CO_3^=$, see Appendix 1.

inorganic carbon in the mixed layer, ΣC_m, is then

$$h\frac{D_g}{Dt}\Sigma C_m = k_0 v_e(p^{\text{atm}}_{\text{CO}_2} - p_{\text{CO}_2}) - \wedge\left(w_{ek} + \frac{D_g h}{Dt}\right)(\Sigma C_m - \Sigma C_{th}) - h_{ek}v_{ek}\frac{\partial \Sigma C_m}{\partial y}. \quad (3)$$

The last term represents the contribution of the horizontal transfers of carbon in the Ekman layer which, we will show, make important contributions. The horizontal Ekman flow is assumed confined to a thin layer, $h_{ek} < h$, and wind-stress acts only in the zonal direction.

The remainder of the column comprises the inviscid, stratified thermocline, and there the dissolved inorganic carbon, ΣC_{th}, evolves according to

$$\frac{D_g}{Dt}\Sigma C_{th} + w_{ek}\frac{\partial}{\partial z}\Sigma C_{th} = 0. \quad (4)$$

The controlling equations, (3) and (4), require knowledge of the mixed-layer depth, temperature and salinity fields, both to delineate the separate regimes and to calculate the chemical equilibration coefficients. The mixed-layer depth, temperature and salinity could be calculated explicitly using a mixed-layer model. However, in this investigation we prefer to *impose* plausible seasonal cycles of mixed-layer depth and temperature. Since the leading influence on the chemical balances is temperature we fix the salinity at a constant 36.5 psu, appropriate to the surface waters of the subtropical gyre.

In the following experiments, the Lagrangian model is used to examine the sensitivity of the carbon cycle to different mixed layer temperature and depth cycles in the absence of biological feedbacks.

b. Gyre circuits of a water column

We explore the interactions of dynamical and chemical effects on the carbon distribution in the column by imposing a history of physical properties that a column might experience if it repeatedly circuited the subtropical gyre. Mixed-layer ΣC is determined by integrating (3), and the profile of ΣC in the thermocline is determined by integrating (4).

The column is now taken on a grand tour of the subtropical gyre (see schematic, Fig. 2(a)). The imposed variations of mixed layer depth and temperature are displayed in Figures 2(b) and 2(c).

The circuit is separated into three regions: 1. *The Subduction Region:* The interior of the subtropical gyre is the primary site of subduction (see Marshall *et al.,* 1993). Here there are meridional gradients in temperature, mixed layer depth and a strong seasonal cycle. In the northern part of this region the mixed layer is cold and deep in winter, and warm and shallow in summer. Horizontal currents are weak and the column spends 8 years in this portion of the circuit. 2. *Low Latitudes:* The column drifts westward for 3 years experiencing shallow, warm mixed layers, with small seasonal amplitudes. 3. *The Gulf Stream:* The column enters the swift, northward flowing western boundary current, and arrives a year later to deep winter mixed layers at the exit of the Gulf Stream. This circuit of

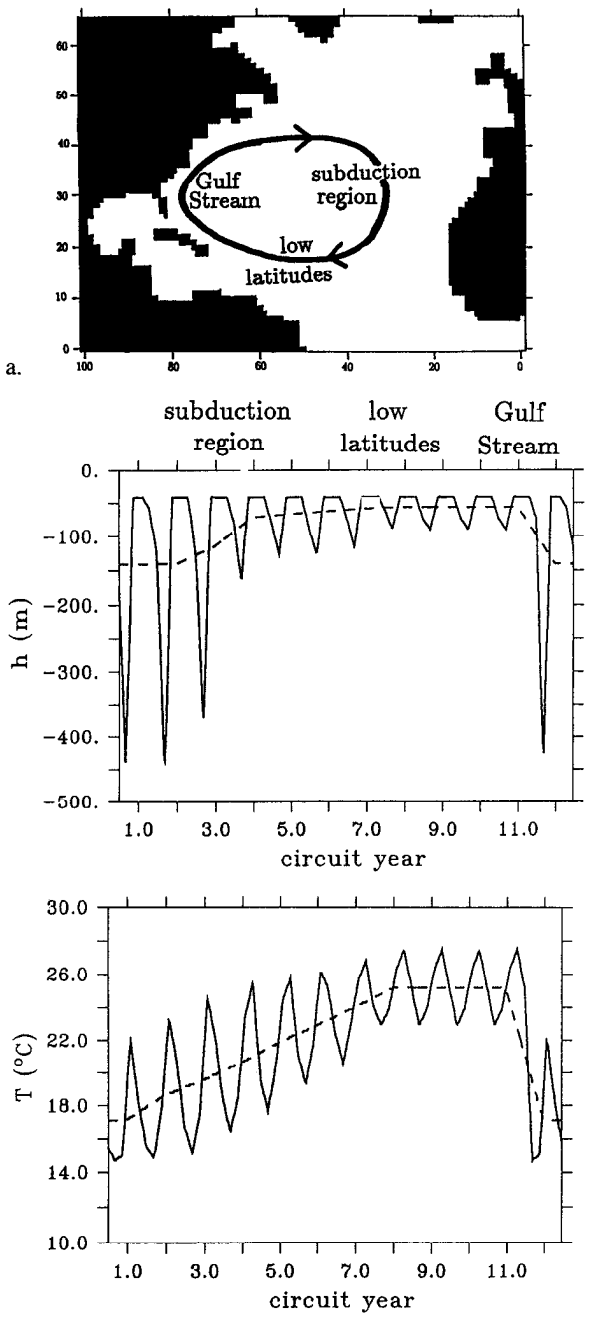

Figure 2. (a) Schematic of the assumed trajectory of Lagrangian column as it circuits the gyre; (b) Imposed mixed layer depth for single circuit of gyre; (c) Imposed mixed layer temperature for single circuit of gyre. The circuit is divided into three conceptual regions. The temporal trends for the mixed layer displayed in (b) and (c) start at the beginning of the subduction region, as the column begins its southwards branch of the circuit.

the gyre is completed in twelve years. The carbon model is integrated over several circuits of the gyre until a steady, repeating cycle in the ΣC profile is achieved.

c. The influence of Ekman advection

We now use the Lagrangian model to illustrate the mechanisms by which the subtropical gyre acts as a vertical pump of carbon into the ocean. In all these experiments, mixed-layer properties appropriate to the seasonally varying case have been imposed, as depicted in Figure 2.

Three experiments are discussed:

- Case 1. $w_{ek} = 0$, $v_{ek}(\partial \Sigma C_m/\partial y) = 0$. The column is isolated from its surroundings. The vertical structure is set entirely by subduction and entrainment, and exchanges with the atmosphere. In the steady state there is no net flux of carbon across the sea surface over one gyre circuit.
- Case 2. $w_{ek} = -50$ m year^{-1}, $v_{ek}(\partial \Sigma C_m/\partial y) = 0$. Ekman pumping is represented, so the column can communicate with the deeper ocean. Net fluxes of carbon across the sea surface are possible over gyre circuits. Lateral fluxes in the Ekman layer are assumed negligible.
- Case 3. $w_{ek} = -50$ m year^{-1}, $v_{ek}(\partial \Sigma C_m/\partial y) \neq 0$. Lateral fluxes in the Ekman layer are represented in the following idealized manner:

$$v_{ek}\left(\partial \Sigma C_m/\partial y\right) = -0.3 \times 10^{-12}\ \mu\text{mol kg}^{-1}\text{s}^{-1}, \text{ northern half of gyre}$$

$$0.6 \times 10^{-12}\ \mu\text{mol kg}^{-1}\text{s}^{-1}, \text{ southern half of gyre.}$$

These broad estimates are obtained using typical observed Ekman flow velocities and surface gradients of ΣC.

The sequence of events as the column circuits the gyre, at steady state, is depicted in Figure 3, which shows end of winter ΣC profiles from case 1, at three selected locations in the gyre. On leaving the subduction region, the seasonal boundary layer of the column is carbon rich, having recently experienced several consecutive winters with deep, cool mixed layers, which absorb CO_2 from the atmosphere. In the low latitude region this carbon-rich column is overlain by a thin, warm mixed layer, which outgasses to equilibrium with the atmosphere. The rapid transit northward in the Gulf Stream brings the column back into the subduction region where deep winter convection occurs on a timescale faster than air-sea exchange can equilibrate carbon to the new, cooler mixed layer temperatures. Consequently, the carbon-depleted, tropical mixed layer water is mixed down through the column, leaving a deep seasonal boundary layer which is depleted in carbon relative to the local equilibrium with the atmosphere. The negative anomaly in ΣC is then eroded in successive seasons during the equatorward drift in the subduction region as carbon is absorbed through the sea surface.

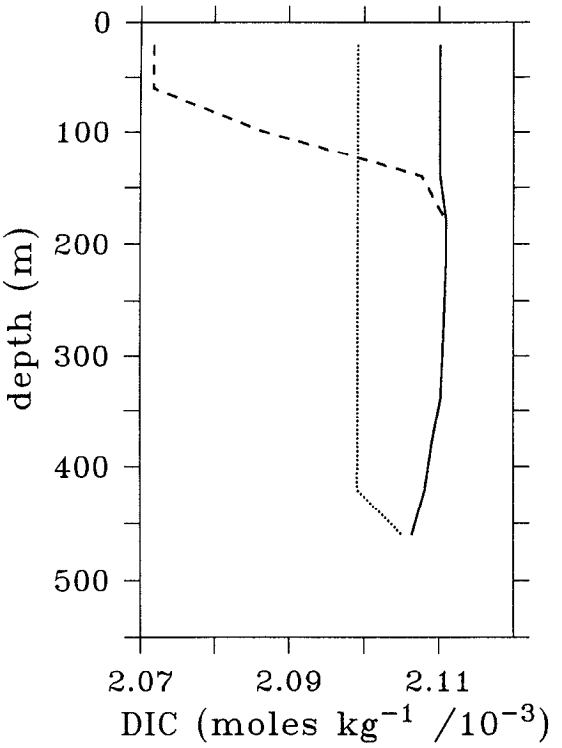

Figure 3. March vertical profiles of ΣC (mmoles kg^{-1}) from case 1, the Lagrangian experiment without Ekman pumping. The *solid line* is from year 4 of the circuit, in the latter part of transit through the subduction region. The seasonal boundary layer is cool and rich in carbon throughout. The *dashed line* is from year 9 of the circuit, in the lower latitudes of the gyre. Warm, shallow mixed layers have outgassed CO_2 to the atmosphere, but overlay the deep carbon rich column created in the subduction region. The *dotted line* is from year 12 of the circuit, following the rapid transit through the Gulf Stream. Deep convective mixing at mid-latitudes has mixed the surface ΣC anomaly created in the low latitudes through the column, leaving it relatively depleted in ΣC compared to profile (i), and undersaturated with respect to the local equilibrium. The deficit is made up during years 1 to 3 as CO_2 is absorbed from the atmosphere.

In Figure 4 we present the time-integrated air-sea flux of CO_2 as the column circuits the gyre for cases 1, 2 and 3. The integrated flux across the sea surface exactly mirrors the trends in the total burden of carbon over the column. The flux is set to zero at an arbitrary initial point (beginning of circuit, year 1), and accumulated over each gyre circuit.

For case 1, with no Ekman transports, there is no net flux across the sea surface over a gyre circuit, because the column is isolated from the adjacent waters, both laterally, and from below. In the Gulf Stream region we see absorption of carbon by the ocean due to local cooling. This oceanic uptake of carbon extends over the interior subduction region, since the equilibration period for carbon is an order of magnitude longer than that for heat.

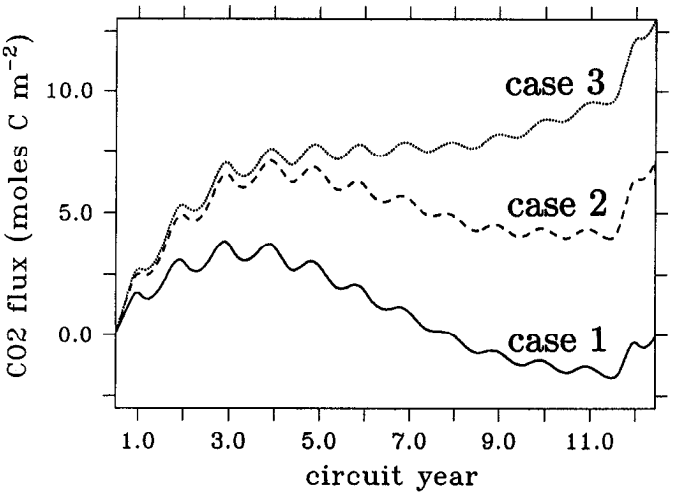

Figure 4. Air-sea flux of carbon integrated around the Lagrangian circuit (moles C m^{-2}). This is equivalent to the change in total column carbon content. A positive value at the end of the circuit indicates a net uptake of carbon from the atmosphere. *Case 1:* No Ekman transports. Since there is no communication with water surrounding the column, or beneath the deepest mixed layer, the circuit integral flux is zero. Gulf stream cooling promotes uptake of carbon by the ocean (positive gradient), which continues through the subduction region. Warming of the mixed layer promotes outgassing in the latter part of the subduction region and low latitudes. *Case 2:* $w_{ek} = -50$ m year^{-1}, $v_{ek}(\partial \Sigma C_m/\partial y) = 0$. Ekman pumping pushes the subducted, carbon rich, waters into the main thermocline, enabling a net uptake of carbon over the gyre. *Case 3:* $w_{ek} = -50$ m year^{-1}, parameterized $v_{ek}(\partial \Sigma C_m/\partial y)$ (see text). Lateral Ekman transports play a significant role in the balance at low latitudes, enhancing the net circuit solubility pump.

However, increasing mixed layer temperature in the subduction region and at low latitudes ultimately leads to outgassing in the shallow mixed-layers, reversing the trend.

In case 2, Ekman pumping acts to subduct cool, carbon rich water from deep winter mixed layers of the northern part of the subtropical gyre (see Fig. 3) down into the main thermocline, inducing a net flux of carbon into the ocean over each circuit. The flux of carbon subducted out of the seasonal boundary layer and into the main thermocline, is balanced by a net flux of carbon across the sea surface. There remains, however, a net annual outgassing over the southern flank of gyre, witnessed by the negative gradient in the accumulated carbon curve.

In case 3, both horizontal and vertical Ekman fluxes of carbon are included. There is a further enhancement of the net absorption of carbon across the sea surface into the gyre. This is a consequence of the poleward flux of warm, low ΣC waters in the Ekman layer on the southern flank of the gyre, which induces a flux of CO_2 into the ocean even in regions where the warming of surface layers (following a geostrophic parcel) would imply outgassing. There is now an overall flux of carbon *into the ocean,* over the whole circuit.

To summarize, three distinct regimes are identified (see Fig. 2(a)):

The Gulf Stream. There is rapid polewards advection, with cooling and absorption of carbon from the atmosphere. Due to the long timescale of carbon equilibration compared to the cooling, the low ΣC water from the tropics is mixed down into deep mixed-layers before equilibrium can be reached.

The Subduction Region. The deep seasonal boundary layer is still undersaturated due to the rapid passage through the Gulf Stream, and uptake of carbon from the atmosphere continues during the equatorward passage in the geostrophic flow. The mixed-layer shoals towards the equator, leading to enhanced subduction of the cool, carbon rich waters.

Low latitudes. The shallow and warm mixed-layers quickly equilibrate with the atmosphere. Lateral fluxes of low ΣC tropical waters in the Ekman layer are significant, reducing surface p_{CO_2}, and promoting further uptake of carbon by the ocean.

In the following section, we explore the role of the seasonal cycle in setting the efficiency of the carbon pump.

d. The influence of the seasonal cycle

The seasonal cycle may influence the rate of transfer of carbon into the main thermocline and across the sea surface in two ways. Firstly, the rate of subduction of mass in the subtropical gyre is largely set by the meridional slope of the winter mixed layer base (Marshall *et al.,* 1993). Secondly, the selection of end-of-winter mixed layer properties for subduction (Stommel, 1979; Williams *et al.,* 1995) suggests a bias toward high ΣC values, associated with cooler, winter waters. We now use the idealized model developed above to explore the sensitivity of the air-sea flux of carbon to these features of the seasonal cycle.

Three further experiments were performed with the same parameters as in the seasonally varying case 3 above:

- Case 4. Forced with annually smoothed mixed layer depth and temperature sequences (Fig. 2, dashed lines).
- Case 5. Forced with annually smoothed mixed layer depths and seasonally varying mixed layer temperatures.
- Case 6. Forced with seasonally varying mixed layer depths and annually smoothed temperatures.

The net circuit contributions from lateral Ekman fluxes are the same in each experiment. Figure 5 shows the resulting cumulative air-sea flux curves from these scenarios, along with that from the reference seasonal experiment, case 3. Striking differences are evident in the air-sea fluxes between the annual mean, case 4, and seasonal, case 3, experiments. The seasonal case has absorbed ~50% more carbon from the atmosphere. This is balanced by an increased flux through the lower boundary of the model. The two curves differ most in the subduction region where, with a seasonal cycle, the column continues to absorb carbon from the atmosphere for substantially longer periods compared to the annual mean case.

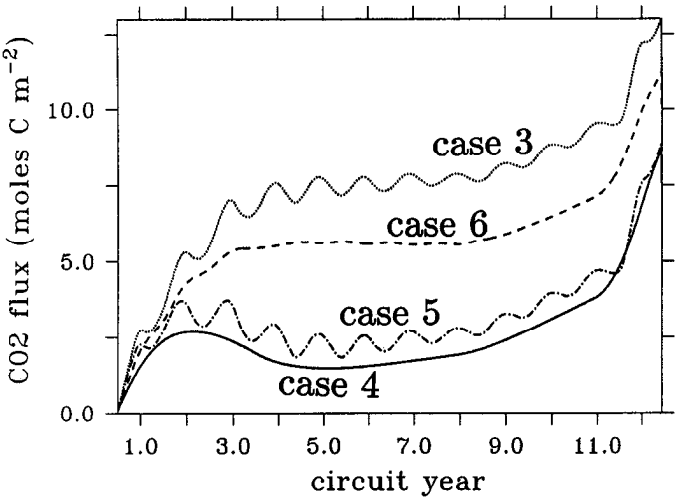

Figure 5. Air-sea flux of carbon integrated around the Lagrangian circuit (moles C m^{-2}, as in Fig. 4). These cases illustrate the role of the seasonal cycle in controlling the net solubility pump over the gyre. Model parameters follow the reference *Case 3* (also shown in Fig. 4) with the following modifications: *Case 4:* As in case 3, but forced with annually smoothed mixed layer temperature and depth (Fig. 2). The "annual mean" case has a substantially weaker solubility pump over the gyre. *Case 5:* As in case 3, but forced with annually averaged mixed-layer depths, and seasonal mixed layer temperatures (Fig. 2). Deep winter mixed-layers and strong meridional gradients are missing, reducing the net solubility pump to that of the fully annually forced case. *Case 6:* As case 3, but forced with seasonal mixed-layer depths, and annually smoothed temperatures. While the solubility pump is close to that of the fully seasonal case some reduction occurs due to the loss of the temperature driven annual cycle. The subduction process selects end-of-winter water properties (high ΣC in the fully seasonal case).

The reasons for this difference are twofold, and can be illustrated by the curves corresponding to cases 5 and 6.

Firstly, the increased slope of the deepest mixed layer base in the seasonal experiments allows the atmosphere to influence a deeper layer of water at high latitudes, demanding a larger flux of carbon from the atmosphere. The enhanced gradient in mixed layer depth drives a greater subduction rate, removing much of the column of cool, carbon rich water from contact with the atmosphere. The local net air-sea flux balances this subduction of carbon. Compare, for example, case 5 with a smoothed mixed-layer depth and the reference seasonally-varying case 3. In case 5, reducing the high latitude mixed-layer depths, and hence the meridional gradient, leads to the net flux over the circuit being less than that in case 3, and instead is close to that of the annual average experiment, case 4. We see then, that the mixed-layer topography is of great importance in setting the efficiency of the solubility pump.

Secondly, the seasonal cycle preferentially transfers the end-of-winter properties of the mixed layer into the main thermocline (Stommel, 1979; Williams *et al.,* 1995). While one

can anticipate that the seasonal amplitude of mixed-layer ΣC is heavily damped due to its long equilibration period ($\sim$ years), there are still seasonal amplitudes in ΣC reaching order 10 μmol kg^{-1}. This is sufficiently large to enhance the subduction of carbon by up to 10 percent over a gyre circuit (the ratio of seasonal amplitude in ΣC to the cross-gyre variation in ΣC). Case 6 (Fig. 5) illustrates the contribution of seasonal bias; it has no seasonal cycle in temperature, thus no significant seasonal selection of subducted properties. The net uptake of carbon over the circuit is indeed reduced by some 10%. However, the combination of temperature and mixed-layer depth cycles reduces the temperature bias somewhat in the fully seasonal case, since re-entrainment of undersaturated water in the winter further damps the seasonal variations of ΣC in the subduction region.

In summary, we have shown that the flux of carbon into the subtropical gyres is significantly influenced by the seasonal cycle. The largest effect of the cycle is its control of the slope of the winter mixed-layer base, which enhances the subduction rate by as much as a factor of two. There is a lesser effect through the selection of winter mixed-layer properties for subduction.

These results suggest that a model with a seasonal cycle should be used in studies of the carbon cycle if one is interested in simulating the magnitudes and patterns of air-sea fluxes in the gyres correctly. However, ocean GCMs driven by annual mean fluxes are often used in ocean carbon cycle studies. To the extent that they reproduce the end-of-winter mixed layer depths (which they do reasonably well), the major effects of the seasonal cycle on the subduction rate, and transfer of carbon, are captured in such steady models. Annual mean models do not, however, produce the correct *T/S* structure and, because of temperature bias, have a tendency to slightly underestimate the uptake of CO_2 from the atmosphere.

3. An abiotic carbon cycle model of the North Atlantic

The Lagrangian model of the previous section illustrates some of the mechanisms by which the ocean circulation impacts on the exchange of carbon between ocean and atmosphere. We now present experiments performed with a much more complicated geochemical model of the North Atlantic. Firstly, the model is integrated in a thought experiment without any advection or diffusion. Secondly, the model is integrated with advection and diffusion, together with plausible lateral boundary conditions for the North Atlantic.

a. The transport model

The North Atlantic model in the advective integration is driven by off-line velocity fields (horizontal; u, v and vertical; w) from the 1.0° × 1.2° CME general circulation model of Bryan and Holland (1989) based on the GFDL general circulation model; the off-line tracer transport model is described in Williams *et al.* (1995), and outlined here in Appendix 2. Model fields are stored every three days providing a fully resolved seasonal cycle for the tracer model. Temperature and salinity fields, also from the CME model, provide density

profiles, from which mixed layer depths are diagnosed. In the experiment discussed here, the domain of the tracer model is restricted to the upper 1600 m of the ocean.

The evolution of ΣC in the mixed layer is determined as a function of air-sea and entrainment fluxes, along with the horizontal and vertical advective fluxes, and horizontal diffusion representing eddy transfers. The distribution in the thermocline is found as an "advection-diffusion" problem, driven by subduction from the mixed-layer. The mixed layer is assumed vertically homogeneous with respect to tracers at all times.

The parameterizations of air-sea exchange and inorganic chemistry are the same as those employed in the Lagrangian experiments. A spatially and temporally uniform piston velocity of 20 cm hr^{-1} is chosen. Sensitivity to the piston velocity has been discussed by Sarmiento *et al.* (1992), who do not find it to be a critical parameter in perturbation CO_2 model studies. Atmospheric partial pressure, $p^{atm}_{CO_2}$, is imposed without long-term trends at an arbitrary value of 350 ppmv. Alkalinity at the surface is specified as a linear function of salinity, following Brewer *et al.*'s (1986a) diagnosis of North Atlantic observations.

b. Boundary conditions

Fluxes through the open boundaries of the model are dealt with by prescribing the ΣC profile at those boundaries. Observed profiles close to the Equator (from GEOSECS; Bainbridge, 1981) and 65N (TTO; Brewer *et al.,* 1986b) are used to infer appropriate profiles of ΣC at the Equator and 65N. Since the model only represents the mechanisms of the solubility pump, the ΣC contribution from the biological pumps is, as far as possible, removed from the observed profiles by applying the method of Brewer (1978).

$$\Sigma C_{sol} = \Sigma C_{obs} - \frac{1}{2}(TA_{obs} - TA_s) - \frac{115}{106} R(O_{2,obs} - O_{2,s}) \tag{5}$$

Here ΣC_{sol} is the dissolved inorganic carbon component due to the solubility pump. Subscripts "obs" indicate observed quantities. TA_s and $O_{2,s}$ are the titration alkalinity and dissolved oxygen concentration in the mixed layer at the time of subduction. The Redfield ratio, $R = 0.74$, carbon-to-oxygen, is taken from Takahashi *et al.* (1985). TA_s and $O_{2,s}$ are determined as functions of the observed temperature and salinity. It is assumed that; (i) away from the mixed-layer the ocean is adiabatic, (ii) the imposed North Atlantic surface alkalinity/salinity relationship (see Appendix 1) is appropriate wherever the sampled waters were subducted, and (iii) that oxygen is always at equilibrium with the atmosphere in the mixed-layer. These assumptions, and the fact that the observations are a snapshot of a transient system, limit the quantitative accuracy of this specification of the boundary conditions. However, the imposed boundary profiles of ΣC, have realistic vertical structures, where ΣC increases with depth, appropriate to the solubility pump component in the North Altantic. This is evident in the section shown in Figure 9 from the advective experiment.

Four profiles from the GEOSECS expedition (station numbers 42, 46, 109, and 111) were analyzed and averaged to provide the profile at the equatorial boundary of the model.

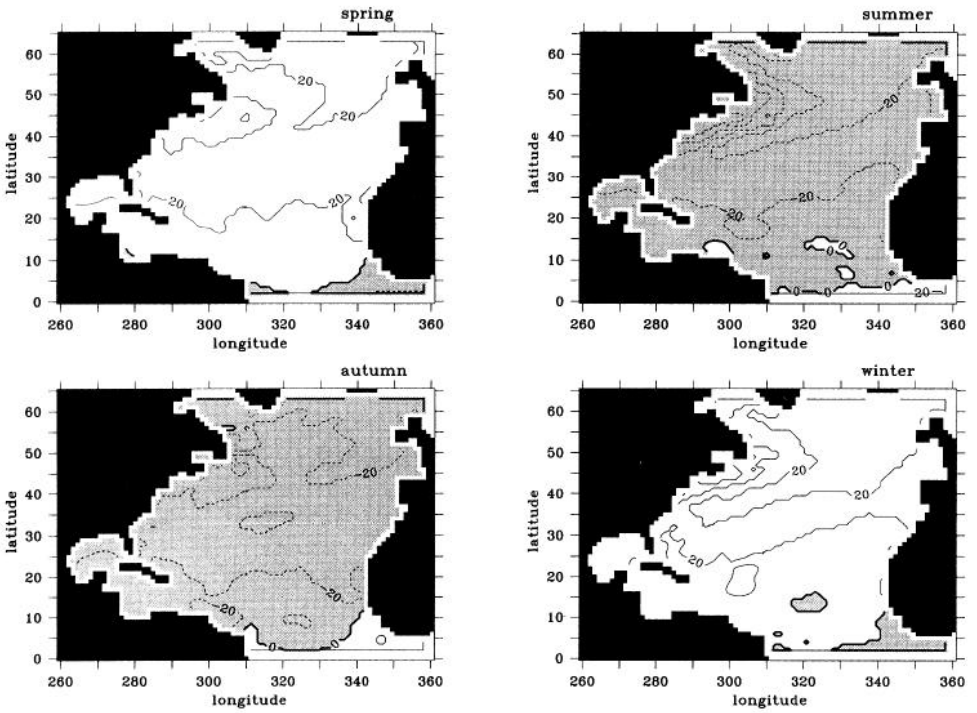

Figure 6. Seasonal snapshots of the atmosphere-ocean difference in p_{CO_2} (microatmospheres) in the nontransport, thought experiment; shading denotes outgassing. The temperature cycle in the model leads to an ocean uptake of CO_2 in the winter and spring, and outgassing over the summer and autumn. As the model is integrated to equilibrium without any advection, at every grid-point the annual flux is zero.

Eight stations from the TTO experiment (station numbers 160, 161, 163, 164, 193, 195, 197, 198) provide the data for the northern boundary condition.

A uniform initial condition of 2100.0 μmol kg^{-1} throughout the basin is chosen, and the model is integrated to a steady repeating annual cycle. Using the basin total carbon loading as an indicator, the model comes to equilibrium after some 200 years of integration. Diagnostics are shown from the 250th year of the integration.

c. Static, thought experiment

In order to illustrate the role of transports, we consider an idealized limit where there is no advection or diffusion of carbon in the GCM. The surface carbon reaches a local equilibrium with the overlying atmosphere with the surface ΣC set by the temperature structure and cycle in the upper waters, in the manner of a grid of static, one-dimensional models. There is a strong seasonal reversal in the air-sea p_{CO_2} difference and hence the air-sea flux over the domain (Fig. 6). There is an influx of CO_2 into the ocean during winter and spring over the entire basin, and conversely an outgassing of CO_2 from the warm

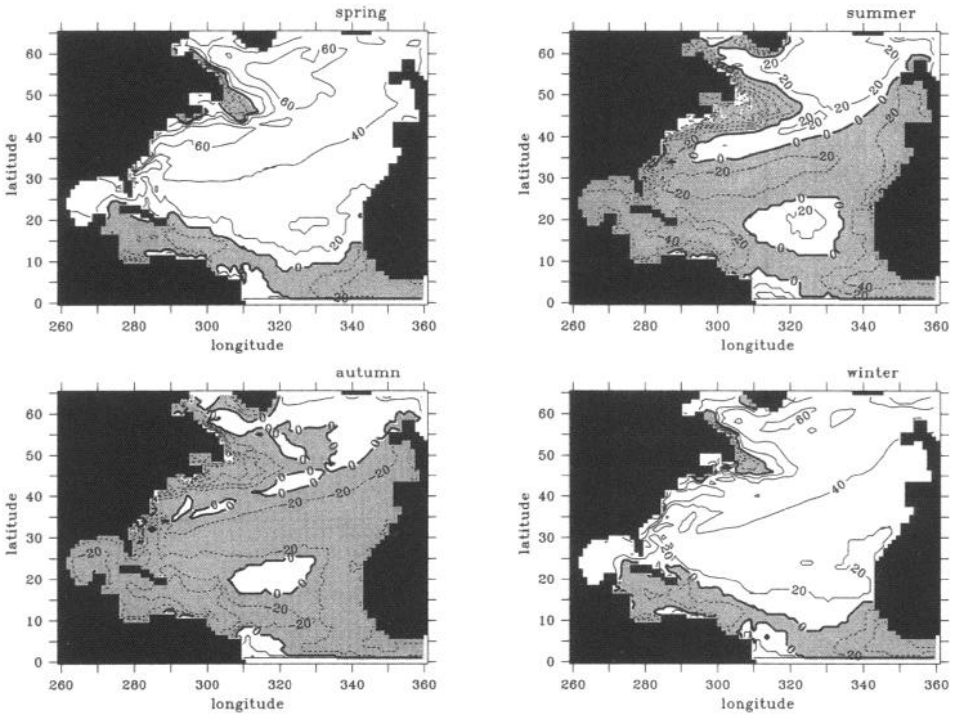

Figure 7. Seasonal snapshots of the atmosphere-ocean difference in p_{CO_2} (microatmospheres) in the advective experiment over the North Atlantic. There is a similar seasonal cycle to the non-advective case (Fig. 6), but there is now a net annual flux into the ocean over the subpolar gyre and over most of the subtropical gyre, and with an annual outgassing over the tropics.

mixed-layers in summer and autumn. Note that this marked seasonal cycle illustrates the difficulty of estimating the annual flux of CO_2 through the sea surface from observations, particularly as the observations are biased to the summer.

In this nonadvective limit, the annual air-sea flux is exactly zero at every grid-point, as the model has been integrated to equilibrium. Thus, the existence of an annual air-sea flux may be viewed as resulting from physical or biological processes taking the ocean away from this *local* equilibrium with the atmosphere. In the next experiment, we investigate the role of the dynamics in controlling the air-sea fluxes of carbon.

d. Advective experiment for the North Atlantic

i. Air-sea fluxes of carbon dioxide. The geochemical model is now integrated with advection and diffusion of carbon included. The seasonal cycle in the atmosphere-ocean p_{CO_2} difference in this advective case is shown in Figure 7. Again there is a general influx of CO_2 during winter and spring, and an outgassing during summer and autumn over most of the domain (compare with the non-advective case shown in Fig. 6). Thus, the temperature cycle is still the dominant process controlling the seasonal cycle in the air-sea flux of CO_2

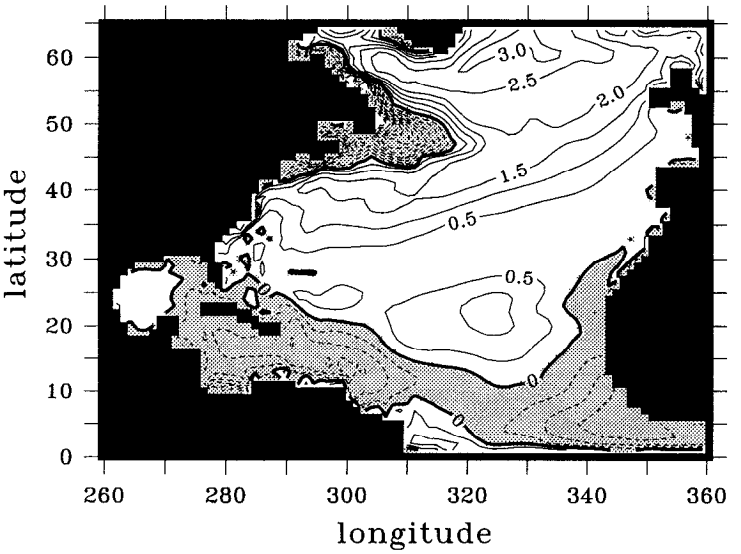

Figure 8. Annually integrated air-sea flux of CO_2 in the advective experiment over the North Atlantic. Fluxes are in moles m^{-2} $year^{-1}$, positive denotes air to sea flux. There is an overall surface uptake of carbon over the entire North Atlantic, which balances the export of carbon-rich, cold water through the open, lateral boundaries by the thermohaline circulation.

in this abiotic experiment. However, the advection of carbon does modify the spatial patterns of p_{CO_2} leading to an annual *influx* of CO_2 to the oceans over most of the subpolar and subtropical gyres, and an outgassing over the tropics, which is apparent in the seasonal and annual-mean plots (Figs. 7 and 8). The annual air-sea flux is acting to offset the effect of advection and attempting to restore the surface ΣC back toward the local equilibrium value. For example, the outgassing in the tropics is due to the upwelling of colder, carbon-rich water there, which increases the surface carbon above that of the local equilibrium value.

The pattern of the annual air-sea flux of carbon over the subtropical gyre (Fig. 8) appears to be broadly consistent with the predictions from the idealized Lagrangian model (Fig. 4, case 3). There is a net annual air-to-sea flux of carbon over almost the entire subtropical gyre, with fluxes of the order of 0.5 to 1.5 moles m^{-2} $year^{-1}$; magnitudes consistent with observations (Tans *et al.,* 1990) and published carbon cycle models (e.g., Bacastow and Maier-Reimer, 1990). The largest fluxes are in the subduction region, where deep winter mixed-layers absorb CO_2 from the atmosphere in response to upstream cooling of the water column in the Gulf Stream. There is also a significant absorption of carbon by the ocean in the southern half of the subtropical gyre due to the polewards Ekman flux there.

Integrating over the whole model domain, there is a net surface influx of carbon since the uptake over the subtropical and subpolar gyres dominates over the outgassing in the tropics. This net surface uptake of carbon over the North Atlantic model is a consequence

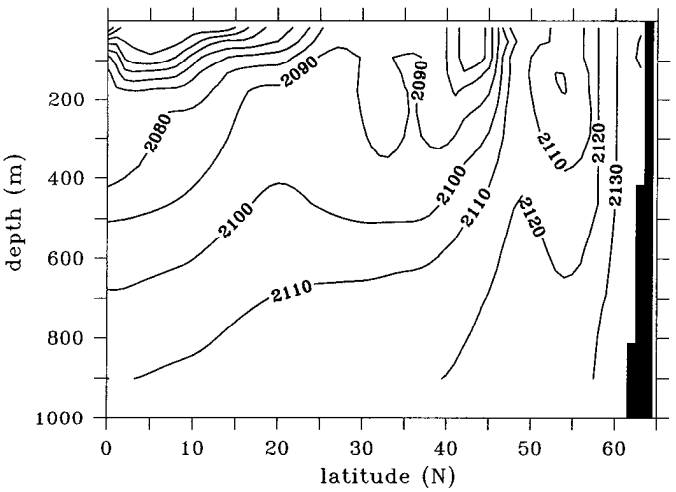

Figure 9. Model section at 40W of ΣC (μmol kg^{-1}) in January at steady state for the advective experiment over the North Atlantic.

of the large-scale thermohaline circulation. Buoyancy forcing drives an overturning circulation, which exports cold water at depth out of the North Atlantic and imports warm surface water through the open, lateral boundaries. This net outflux of cold water leads to a corresponding outflux of carbon from the basin balanced, at steady state, by the net surface input of CO_2 over the North Atlantic domain.[4]

ii. Carbon distribution. At steady state, the model has a plausible vertical carbon structure, with ΣC increasing with depth and latitude over most of the basin (Fig. 9). Over the upper 500 m, the presence of the wind-driven gyres is evident with lower ΣC in the subtropical gyre where there is a thicker main thermocline (20N to 45N) and higher ΣC in the subpolar gyre where there are weaker vertical gradients. In the upper part of the subtropical gyre, the vertical structure reflects the properties subducted from the mixed layer into the main thermocline. The deeper structures reflect the advection of the imposed lateral boundary conditions into the interior.

The surface ΣC distribution reflects the high solubility at lower temperatures and the influence of the ocean curents (Fig. 10). The gyre circulation moves the surface waters away from a local equilibrium with the atmosphere, inducing the regional net air-sea fluxes seen in Figure 8.

iii. The carbon balance in the surface layer. The annual mean carbon budget is now diagnosed in more detail in order to reveal the relative importance of advection, diffusion,

4. If a biological cycle is incorporated, one expects there to be a further bias toward oceanic uptake of carbon due to the spring and summer drawdown of ΣC into organic matter.

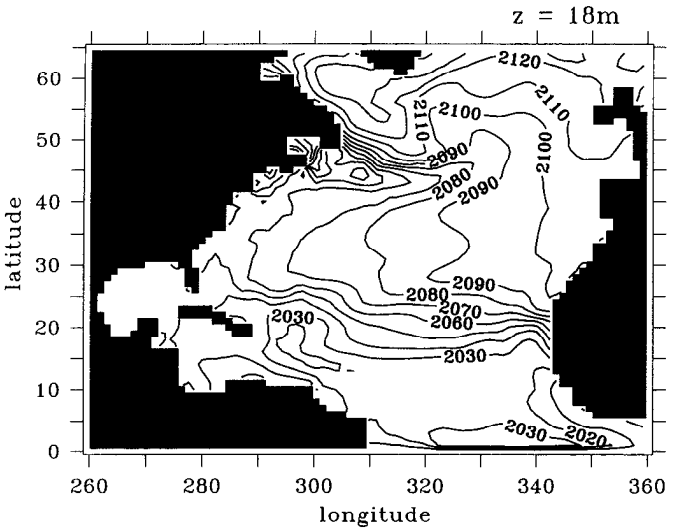

Figure 10. Model surface ΣC (μmol kg^{-1}) in January at steady state for the advective experiment over the North Atlantic.

air-sea exchange, and entrainment. The tendencies due to the individual terms in the tracer equation for carbon are integrated over one annual cycle, and from the surface to 330 m (the seven uppermost model levels), and are shown in Figure 11. The strong seasonal balance between temporal evolution, entrainment and air-sea exchange is averaged out. The diagnostic equation is:

$$\left\langle \frac{\partial \Sigma C}{\partial t} \right\rangle = \underbrace{-\langle \mathbf{U} \cdot \nabla \Sigma C \rangle}_{\text{advection}} + \underbrace{\langle \nabla \cdot (K \nabla \Sigma C) \rangle}_{\text{eddy transfer}} + \underbrace{\langle v_e k_0 (p_{CO_2^{air}} - p_{CO_2}) \rangle}_{\text{air - sea exchange}} + \underbrace{\left\langle \frac{dh}{dt} (\Sigma C_{th} - \Sigma C_m) \right\rangle}_{\text{entrainment}}, \tag{6}$$

where $\langle\ \rangle \equiv \int_0^{1yr} \int_{-330m}^{0} dtdz$. When the model has reached a steady, repeating seasonal cycle, the temporal term (left-hand side) vanishes, and the balance of the remaining terms may be examined.

Over the subtropical gyre, the eddy transfer term (here parameterized by diffusion) is of secondary importance, although in the subpolar gyre, the eddy transfer tendency is of similar magnitude to that of advection (Fig. 11(b)). As we choose to integrate over a layer which is generally thicker than the mixed-layer, entrainment is not very significant in the subtropical gyre (Fig. 11(d)).

The dominant balance in the annual mean budget is therefore between advection and air-sea exchange (Fig. 11(a) and (c)). In the subtropical gyre, advection tends to reduce ΣC, leading to undersaturation, and inducing uptake of atmospheric CO_2. In the northern half of

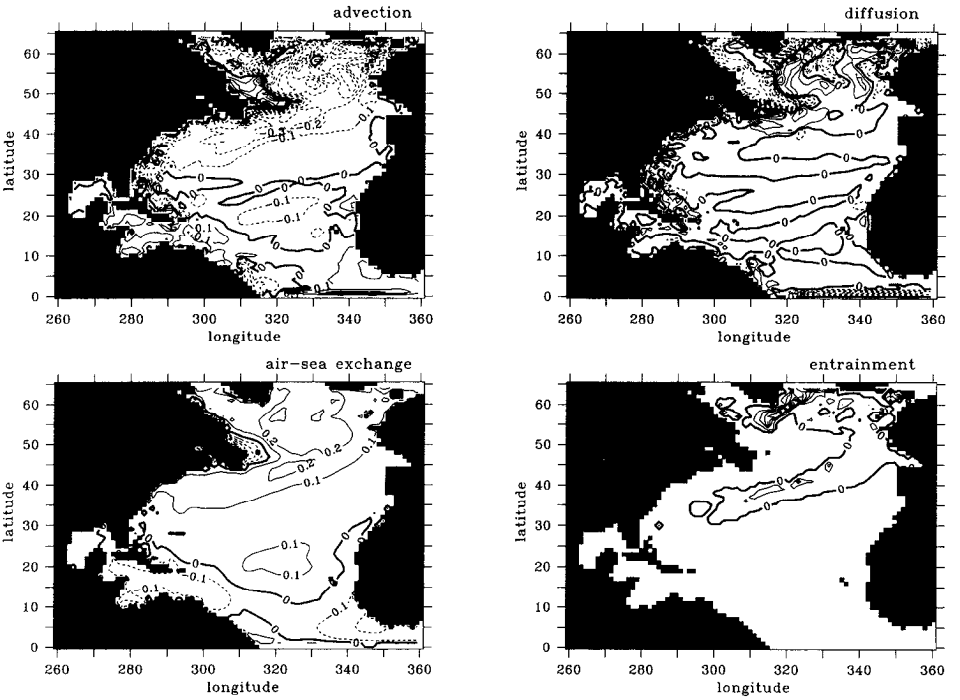

Figure 11. Steady state model diagnostics for the advective experiment over the North Atlantic. Annually averaged tendencies (mol $kg^{-1}s^{-1}/10^{-12}$), integrated over the upper 330 m of the model. Positive values indicate a tendency to increase ΣC locally. The sum of the individual tendencies depicted is zero everywhere, since the model is at steady state. Depicted are (a) advective tendency; (b) diffusive tendency; (c) air-sea flux of CO_2, and (d) entrainment during convective mixing.

the gyre this is primarily due to the outflow of low ΣC waters from the Gulf Stream. In the southern part of the gyre, there is a strong uptake of atmospheric carbon prompted by the transport of warm, low carbon waters from the tropics in the Ekman layer. In the following section we diagnose the roles of the geostrophic and Ekman advection.

iv. Geostrophic and Ekman advection. The advective transfer of carbon is now separated into geostrophic and Ekman components. Monthly Ekman flow fields are determined using the Hellerman and Rosenstein (1983) data set, which was used to drive the dynamical model, such that $h_{ek}u_{ek} = -\tau_y/\rho f$ and $h_{ek}v_{ek} = \tau_x/\rho f$. The Ekman layer depth, h_{ek}, is assumed equivalent to the uppermost model layer depth, and w_{ek} is found by continuity, allowing us to deduce the Ekman transports of carbon. The geostrophic advection is then taken to be the total advection minus the Ekman component, which assumes there is no other ageostrophic flow. The vertical component of Ekman velocity, w_{ek}, is assumed constant in the surface waters below the Ekman layer for the purpose of this diagnostic.

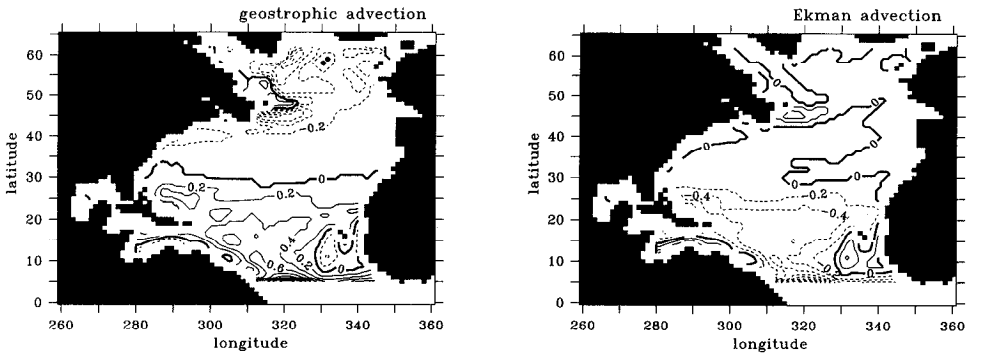

Figure 12. Annual average model tendencies due to (a) geostrophic advection, and (b) Ekman advection, over the upper 330 m at steady state. Positive values indicate a tendency to increase ΣC locally. Note the dominance of Ekman transports in the southern part of the subtropical gyre, which override the positive tendency from the southward geostrophic transports. In the northern part of the gyre the geostrophic outflow from the Gulf Stream dominates, with a supporting contribution from Ekman transports.

In the model, geostrophic advection leads to a supply of low ΣC water to the northern half of the subtropical gyre, and the subpolar gyre (Fig. 12a). This is particularly striking along the path of the Gulf Stream around 42N, 40W. After cooling in the Gulf Stream, the surface waters are somewhat undersaturated compared to the local static equilibrium of ΣC, because the air-sea exchange equilibration timescale ($\sim$ years) is slow compared to the advective timescale. This leads to a negative meridional ΣC gradient in the northwestern part of the gyre (around 35 to 40N). Thus the main influence of geostrophic advection is to reduce the carbon concentration in that area (Fig. 12b).

Ekman advection leads to a supply of low ΣC waters to the southern half of the subtropical gyre, and a supply of high ΣC waters to the tropics and southwest corner of the subtropical gyre (48N, 40W; Fig. 12b).

In the model, geostrophic advection generally dominates over Ekman transfer in the northern half of the subtropical gyre and subpolar gyre, but Ekman transfer dominates in the southern half of the subtropical gyre and in the tropics (compare Figs. 11a and 12a). The net result is that advection generally supplies low ΣC to mid and high latitudes, and high ΣC in the tropics. Thus, there is annual outgassing of CO_2 over the tropics and an influx elsewhere (as shown in Fig. 8).

4. Implications for observed time-series

Michaels *et al.* (1994) derive an annual budget for carbon in the upper ocean at the Bermuda time series location, based on a series of observations at that site (31°50′ N, 64°10′ W). Observations include the local concentrations of dissolved inorganic and organic carbon, particulate organic carbon, and the vertical fluxes of particulate organic carbon. However, the budget does not balance. A summertime decrease in carbon is not

explained by the diagnosed air-sea exchange, vertical pumping, or particulate fallout. Michaels *et al.* (1994) suggest that this could be due to inaccuracies in sediment trap measurements of particulate fallout, or a consequence of lateral advection. However, Michaels *et al.* (1994), referring to unpublished ΣC transects, suggest that the geostrophic advection of ΣC in the Sargasso Sea is unable to close the budget at Bermuda since the meridional gradient of ΣC in that region is positive (N. Bates, personal communication).

Winn *et al.* (1994) obtain similar sets of observations at Hawaii, in the North Pacific subtropical gyre. They find it impossible to close the local upper-ocean carbon budget without invoking lateral advection, and speculate that Ekman transfer of low ΣC waters from the tropics induces a net uptake of CO_2 from the atmosphere at that site.

Both the Lagrangian and GCM models described here show that advection is generally a crucial process in controlling the local carbon budget over the North Atlantic. The models suggest that geostrophic advection dominates over the northern part of the subtropical gyre and Ekman transfer over the southern part. With respect to the Michaels *et al.* (1994) observations, we actually find that both the geostrophic and Ekman terms change sign at Bermuda in the general circulation model (Fig. 12). However, we do not believe that the exact position of the zero line is reliable in the general circulation model, as it is probably sensitive to model forcing and subgrid scale parameterizations. Thus, we believe that some form of advection, including that from the time-mean and time-varying geostrophic or Ekman flows, remain likely candidates to close the carbon budget at Bermuda. However, evaluating the real advective contribution requires a careful three-dimensional evaluation over the year, which is difficult to achieve observationally.

5. Conclusions

The role of dynamics and the seasonal cycle in controlling the carbon distribution over the North Atlantic is examined using a hierarchy of abiotic models. Static, one-dimensional carbon cycle models reasonably capture the *seasonal* variation in surface ΣC and p_{CO_2} through the local balance between temporal evolution, air-sea fluxes and entrainment. However, these terms partly oppose each other over an annual cycle and the dominant balance becomes between advection and the annual air-sea flux. Indeed one-dimensional studies are unable to close the local carbon budget without invoking lateral advection or large observational errors.

A Lagrangian model is used to provide a simple mechanistic representation of the carbon system of the subtropical gyre. The gyre circulation and regional temperature changes lead to the transfer of carbon into the ocean over the whole of the subtropical gyre. Gulf Stream cooling promotes an air-to-sea flux of carbon in the northern part of the gyre and carbon rich waters are subducted there. The subduction of mass is balanced by inflow in the Ekman layers, which in the southern part of the gyre bring warm, carbon-depleted water from the tropical mixed-layer, leading to further uptake of atmospheric CO_2.

The seasonal cycle significantly enhances the gyre's uptake of atmospheric CO_2 in two ways: (i) by the increased gradient in mixed layer depth across the gyre during the winter,

which enhances the subduction of mass and carbon, and (ii) by the selection of winter (cold, ΣC-rich) properties for subduction. The former effect enhances the annual uptake of CO_2 by a factor of more than 50%, while the latter has a smaller impact.

The North Atlantic carbon cycle model shows carbon balances similar to the Lagrangian study. In a nontransport limit, a local equilibrium is reached between the ocean and atmosphere; there is a seasonal cycle in the air-sea fluxes of CO_2, but the annual-mean flux is exactly zero. When advection and diffusion of carbon are included in the GCM, the carbon distribution is moved away from that of a local equilibrium leading to an annual air-sea flux of CO_2. Over most of the subtropical gyre and high latitudes, advection leads to a lower surface carbon for the ocean and an influx of CO_2 to the ocean. Conversely, the upwelling of high carbon waters in the tropics leads to an outgassing of CO_2 there. At the steady state of this model, there is an overall surface influx of CO_2 over the entire basin, which balances the outflux of carbon through the lateral boundaries. This outflux of carbon results from the thermohaline circulation in the modeled Atlantic with an influx of warm, carbon-depleted water near the surface and an outflux of cold, carbon-rich water at depth. Thus, our study of the solubility pump would be modified for another basin, such as the Pacific, due to the contrasting thermohaline circulation there.

This abiotic study has neglected the role of the biological uptake of ΣC in the euphotic zone and export through fallout. Such processes will also modify the carbon distribution and lead to annual air-sea fluxes of CO_2. However, our conclusions concerning the importance of the geostrophic and Ekman advection in controlling the annual air-sea flux of CO_2 on regional scales may still be relevant, although the precise balances might be modified. Local ocean carbon budgets must account for these advective processes if they are to be closed. The transfer by geostrophic eddies may also turn out to be important through their direct transfer or modification of the background circulation, although these effects are currently only crudely parameterized in ocean carbon cycle models.

Acknowledgments. We thank Bill Jenkins, Ed Boyle, John Edmond, Klaus Keller and Tom Haine for helpful discussions. Thanks to Robbie Toggweiler for pointing us to the the BATS time series data and to Nick Bates for discussions concerning that data set. The comments of two anonymous reviewers have prompted significant improvement of this manuscript. This work was supported in part by the Tokyo Electric Power Company, through the TEPCO/MIT Research Program, and NSF Grants OCE-9115915 and OCE-9402308. RGW is grateful for support from the NERC UK WOCE Special Topic GST/02/813.

APPENDIX 1

Modeling inorganic carbon chemistry

The parameterization of air-sea exchange of carbon requires the determination of the partial pressure of CO_2 in the surface ocean. This is a function of the local chemical balance between dissolved carbon species. We determine p_{CO_2} in the scheme outlined below, which follows that of Hoffert *et al.* (1979).

In the aqueous system, dissolved carbon dioxide, CO_2(aq), forms carbonic acid and

dissociates into bicarbonate and carbonate forms:

$$CO_2(aq) + H_2O \rightleftharpoons H_2CO_3 \tag{A1}$$

$$H_2CO_3 \rightleftharpoons H^+ + HCO_3^- \tag{A2}$$

$$HCO_3^- \rightleftharpoons H^+ + CO_3^= \tag{A3}$$

Since dissolved $CO_2(aq)$ and H_2CO_3 are difficult to distinguish it is customary to refer to their combined aqueous concentration, which we represent here by $[CO_2]$.

In modeling the oceanic carbon cycle, we carry dissolved inorganic carbon, ΣC:

$$\Sigma C = [CO_2] + [HCO_3^-] + [CO_3^=], \tag{A4}$$

which is conservative in inorganic reactions and transport processes. However, the parameterization of air-sea exchange requires knowledge of the component concentrations, specifically $[CO_2]$ from which the partial pressure, p_{CO_2}, can be deduced.

The component concentrations may be evaluated if the chemical system is assumed to be locally at equilibrium at all times, a good assumption since equilibrium is reached in a matter of seconds. Equilibrium relations for the inorganic carbon species are defined:

$$\frac{[HCO_3^-][H^+]}{[CO_2]} = k_1 \tag{A5}$$

$$\frac{[CO_3^=][H^+]}{[HCO_3^-]} = k_2 \tag{A6}$$

The coefficients k_1 and k_2 have been determined in laboratory studies by Mehrbach *et al.* (1973) and the results parameterized by Dickson and Millero (1987). In all experiments shown here we use these evaluations of the coefficients. While more recent evaluations may now be considered more accurate (e.g. Goyet and Poisson, 1989), our results are qualitatively unaffected.

Eqs. (10)–(12) are insufficient to close the system. There are three equations but four unknown variables: $[CO_2]$, $[HCO_3^-]$, $[CO_3^=]$, and $[H^+]$. We introduce two further relations to overcome this: Firstly the equilibrium dissociation of water,

$$[OH^-][H^+] = k_w, \tag{A7}$$

where $k_w(T, S)$ is as used by Hoffert *et al.* (1979). Secondly we impose the titration alkalinity, TA,

$$TA = [HCO_3^-] + 2[CO_3^=] + [H_2BO_3^-] + [OH^-] - [H^+]. \tag{A8}$$

Titration alkalinity, TA, places a further constraint on the chemistry by expressing the fact that the system should be electrostatically neutral. Here we also introduce the influence of boron species, which while of secondary importance to carbon species, are the most

significant of the minor components contributors to the alkalinity.[5] We specify surface TA as an empirical function of salinity, S(psu), from the analysis of North Atlantic observations by Brewer *et al.* (1986a):

$$\mathrm{TA}(\mu\mathrm{mol\ kg^{-1}}) = 587.05 + 50.560S. \tag{A9}$$

Evaluating TA from (A9), we are left with seven equations; (A4)–(A8) plus two for boron, and seven unknowns; $[CO_2]$, $[HCO_3^-]$, $[CO_3^=]$, $[H_2BO_3]$, $[H_2BO_3^-]$, $[H^+]$ and $[OH^-]$. By substitution, we reduce the equations to a single expression—a fifth order polynomial in $[H^+]$. The coefficients of the polynomial are functions of ΣC, TA, ΣB, and the equilibration coefficients k_1, k_2, k_b, and k_w. The appropriate root of the polynomial is found numerically (by Newton-Raphson iteration), and the equilibrium component concentrations can be retrieved.

The partial pressure of carbon dioxide in the surface water, p_{CO_2}, which is required for the parameterization of air-sea exchange of CO_2 is then determined by Henry's Law;

$$p_{CO_2} = \frac{[CO_2]}{k_0} \tag{A10}$$

where the coefficient, k_0, is a function of T and S as determined by Weiss (1974).

APPENDIX 2

Tracer integration

Transports of the tracer field, A, are determined by numerically integrating the advection and diffusion equation:

$$\frac{\partial A}{\partial t} + \nabla \cdot (\mathbf{u}A) - \nabla \cdot (K \nabla A) = 0.$$

The tracer integration uses fields of velocity, $\mathbf{u}$, temperature, T, and salinity, S, taken from the CME integration. There are 120 sets of dynamical fields, representing information every 3 days over a single year.

The tracer equation is integrated with an Euler forward time scheme and upstream space differencing, using a timestep of ½ of a day to satisfy the CFL condition. The advective and diffusive fluxes are both set to zero on the coastal boundaries.

The explicit diffusivity, k, is chosen to have a horizontal value of 1000 $m^2\ s^{-1}$ and a zero vertical value. Implicit diffusion from the upward scheme smears the tracer along streamlines with a magnitude of $\frac{1}{2}U\Delta x$, which for a flow of $U \sim 1$ cm s^{-1} and a grid-spacing $\Delta x \sim 100$ km gives an implicit diffusion of 500 $m^2\ s^{-1}$.

5. The equilibration of dissolved boron species is determined in a similar manner to that of the dissolved carbon species. We assume a uniform dissolved inorganic boron concentration, $\Sigma B = 409.0$ μmol kg^{-1}, and T and S dependence of dissociation coefficients as used for the GEOSECS data analysis (Takahashi *et al.*, 1981).

REFERENCES

Bacastow, R. and E. Maier-Reimer. 1990. Ocean circulation model of the carbon cycle. Climate Dyn., *4,* 95–125.

Bainbridge, A. E. 1981. GEOSECS Atlantic Expedition. Volume 1: Hydrographic Data 1972–1973. US Government Printing Office, Washington D.C.

Brewer, P. G. 1978. Direct observation of the oceanic CO_2 increase. Geophys. Res. Lett., *5,* 997–1000.

Brewer, P. G., A. L. Bradshaw and R. T. Williams. 1986a. Measurements of total carbon dioxide and alkalinity in the North Atlantic Oceanin 1981, *in* The Changing Carbon Cycle: A Global Analysis, J. R. Trabalka and D. E. Reichle, eds., Springer-Verlag, New York, 592 pp.

Brewer, P. G., T. Takahashi and R. T. Williams. 1986b. Transient tracers in the oceans (TTO)—Hydrographic data and carbon dioxide systems with revised carbon chemistry data. Carbon Dioxide Information Center, U.S. Department of Energy, Oak Ridge, Tennessee.

Broecker, W. S., and T.-H. Peng. 1982. Tracers in the Sea, Eldigio Press, Lamont Doherty Geological Observatory, Palisades, NY, 691 pp.

Bryan, F. O. and W. R. Holland. 1989. A high resolution simulation of the wind- and thermohaline-driven circulation of the North Atlantic Ocean, paper presented at Hawaiian Winter Workshop: Parameterizations of small scale processes, University of Hawaii, Jan 17–20, 1989. Sponsored by U.S. Office of Naval Research, Hawaiian Institute of Geophysics and Department of Oceanography, University of Hawaii.

Denman, K. L. 1973. A time-dependent model of the upper ocean. J. Phys. Oceanogr., *3,* 173–184.

Dickson, A. G. and F. J. Millero. 1987. A comparison of the equilibrium constants for the dissociation of carbonic acid in seawater media. Deep-Sea Res., *34,* 1733–1743.

Goyet, C. and A. Poisson. 1989. New determination of carbonic acid dissociation constants in seawater as a function of temperature and salinity. Deep-Sea Res., *36,* 1635–1654.

Hellerman, S. and M. Rosenstein. 1983. Normal monthly wind stress over the world ocean with error estimates. J. Phys. Oceanogr., *13,* 1093–1104.

Hoffert, M. I., Y.-C. Wey, A. J. Callegari, and W. S. Broecker. 1979. Atmospheric response to deep sea injections of fossil fuel carbon dioxide. Climate Change, *2,* 53–68.

Iselin, C. O'D. 1939. The influence of vertical and lateral turbulence on the characteristics of waters at mid-depths. Trans. Amer. Geophys. Union, *20,* 414–417.

Marshall, J. C., A. J. G. Nurser and R. G. Williams. 1993. Inferring the subduction rate and period over the North Atlantic. J. Phys. Oceanogr., *23,* 1315–1329.

Mehrbach, C., C. H. Culberson, J. E. Hawley and R. M. Pytkowicz. 1973. Measurement of the apparent dissociation constants of carbonic acid in seawater at atmospheric pressure. Limnol. Oceanogr., *18,* 897–907.

Michaels, A. F., N. R. Bates, K. O. Buessler, C. A. Carlson and A. H. Knap. 1994. Carbon-cycle imbalances in the Sargasso Sea. Nature, *372,* 537–540.

Sarmiento, J. L., J. C. Orr and U. Siegenthaler, 1992. A perturbation simulation of CO_2 uptake in an ocean general circulation model. J. Geophys. Res., *97,* C3, 3621–3645.

Stommel, H. 1979. Determination of watermass properties of water pumped down from the Ekman Layer to the geostrophic flow below. Proc. Nat. Acad. Sci. U.S., *76,* 3051–3055.

Takahashi, T., W. S. Broecker and S. Langer. 1985. Redfield ratios based on chemical data from isopycnal surfaces. J. Geophys. Res., *90,* 6907–6924.

Takahashi, T., R. T. Williams and D. L. Bos. 1981. Carbonate Chemistry; in GEOSECS Atlantic Expedition. Vol. 1. Hydrographic Data 1972–1973, National Science Foundation, Washington D.C.

Tans, P. P., I. Fung and T. Takahashi. 1990. Observational constraints on the global atmospheric CO_2 budget. Science, *247,* 1431–1438.

Weiss, R. F. 1974. Carbon dioxide in water and seawater: The solubility of a non-ideal gas. Marine Chem., *2,* 203–215.

Williams, R. G., M. A. Spall and J. C. Marshall. 1995. Does Stommel's mixed layer 'Demon' work? J. Phys. Oceanogr., *25,* 3089–3102.

Winn, C. D., F. T. Mackenzie, C. J. Carrillo, C. L. Sabine and D. M. Karl. 1994. Air-sea carbon dioxide exchange in the North Pacific subtropical gyre: Implications for the global carbon budget. Global Biogeochem. Cycles, *8,* 157–163.

Woods, J. D. 1985. Physics of thermocline ventilation. Coupled Atmosphere-Ocean Models., J. C. J. Nihoul, ed., Elsevier, 543–590.

Xu, Y.-F. 1990. A Study of the Biogeochemical Cycle of CO_2 in the Ocean Using a Parcel Model. Ph.D. thesis, University of East Anglia, Norwich, U.K., 160 pp.

Xu, Y.-F. and J. S. A. Green. 1996. Modeling the biogeochemical cycle of CO_2 in the ocean using a parcel model. Deep-Sea Res., (submitted).

Received: *24 May, 1994;* revised: *19 March, 1996.*